ADVANCED OPTICAL MATERIALS
www.advopticalmat.de

Polymer-Encapsulated Halide Perovskite Color Converters

*Bas A. H. Huisman and Henk J. Bolink**

An easy process to fabricate highly luminescent and color-pure polymer-encapsulated halide perovskite color converters is reported. Methylammonium lead bromide ($MAPbBr_3$) with an additive of amantadine hydrochloride is prepared by dry mechanochemical synthesis together with an encapsulating polymer. (In this report, poly(methyl methacrylate), polystyrene, and polyethylene oxide are investigated.) The composite material is heated and pressed into a thin disk exhibiting strong luminescent properties. By adjusting the weight percentage of the perovskite in the polymer, the disk can be opaque or transmissive. The disks are stable in air for over 2 months. By inserting a secondary emitter, white light can be obtained by illuminating it with a blue light source.

1. Introduction

Color converters are used to convert incident light to a different color and are widely used in commercial displays. To achieve a wide color gamut for these displays, the color converter needs to have a high color purity. This requires that the emitter has an emission spectrum with a narrow full-width at half-maximum (FWHM). Additionally, it is desirable that the color converter has a high photoluminescence quantum yield (PLQY) to efficiently convert the incoming light.

Metal halide perovskites are well suited as emitters in color converters as they fulfill all requirements above described. They have a high PLQY, a narrow FWHM (<30 nm) leading to a high color purity, and their emission wavelength can be tuned by the composition of the perovskite. Additionally, they have a high absorption coefficient for blue light and the material costs are low.[1–7] These unique properties can make halide perovskites interesting for commercialization in displays.[8,9] Metal halide perovskites are generally prepared using a solvent-based process. Due to the different solubilities of the precursor salts and additives, it is not always trivial to reproducibly control the final composition (and thus the optical properties) of the perovskite-based emitters.[10] Residual solvents have also been reported to affect the perovskite stability and optical properties.[11,12]

Mechanochemical synthesis is an alternative, solvent-free, method to prepare highly luminescent perovskite materials.[13–16] Mechanochemical synthesis has shown the capability to easily adjust the composition or introduce an additive into the system without any extra difficulties for the synthesis itself.[17–19] Some reports describe that mechanochemical synthesis produces more crystalline perovskites compared to similar ones produced via solution processing.[20] It is a reproducible method and it has a high versatility to the final composition, making it a desirable route to prepare color converters.

Most perovskites are known to degrade rapidly when in contact with ambient conditions. To compete with commercial color converters, the stability of perovskite color converters needs to be improved.[21] One way to protect the perovskite from these influences is to shield the perovskite from the environment. Multiple articles have shown that polymers can passivate and protect the perovskite from getting in contact with the environment.[22–25] Due to the solvent-free nature of the process, a wide variety of polymeric materials can be employed as there are no restrictions related to their solubility. Furthermore, the partial substitution of the perovskite with the polymer material can have extra advantages for structuring the color converter.[26–28]

In this paper, we demonstrate the formation of perovskite–polymer composites by mechanochemical synthesis employing amantadine hydrochloride (AmCl)-modified $MAPbBr_3$ perovskite in combination with three polymers; poly(methyl methacrylate) (PMMA), polystyrene (PS), and polyethylene oxide (PEO). The synthesized powders are then pressed into thin disks that have a high PLQY and depending on the perovskite concentration and thickness are transmissive or reflective. These perovskite polymer composites are stable in ambient conditions for over 2 months. This novel solvent-free technique to obtain highly luminescent perovskite–polymer composites in moldable shapes is promising for the preparation of color converters.

2. Results and Discussion

To obtain high-performing color converters, the initial perovskite powder must have a high PLQY. In a previous report by our group, high luminescent $MAPbBr_3$ perovskite powders were obtained by mechanochemical synthesis by introducing AmCl into

B. A. H. Huisman, H. J. Bolink
Instituto de Ciencia Molecular
Universidad de Valencia
C/ Catedrático J. Beltrán 2, Paterna 46980, Spain
E-mail: henk.bolink@uv.es

The ORCID identification number(s) for the author(s) of this article can be found under https://doi.org/10.1002/adom.202202921

DOI: 10.1002/adom.202202921

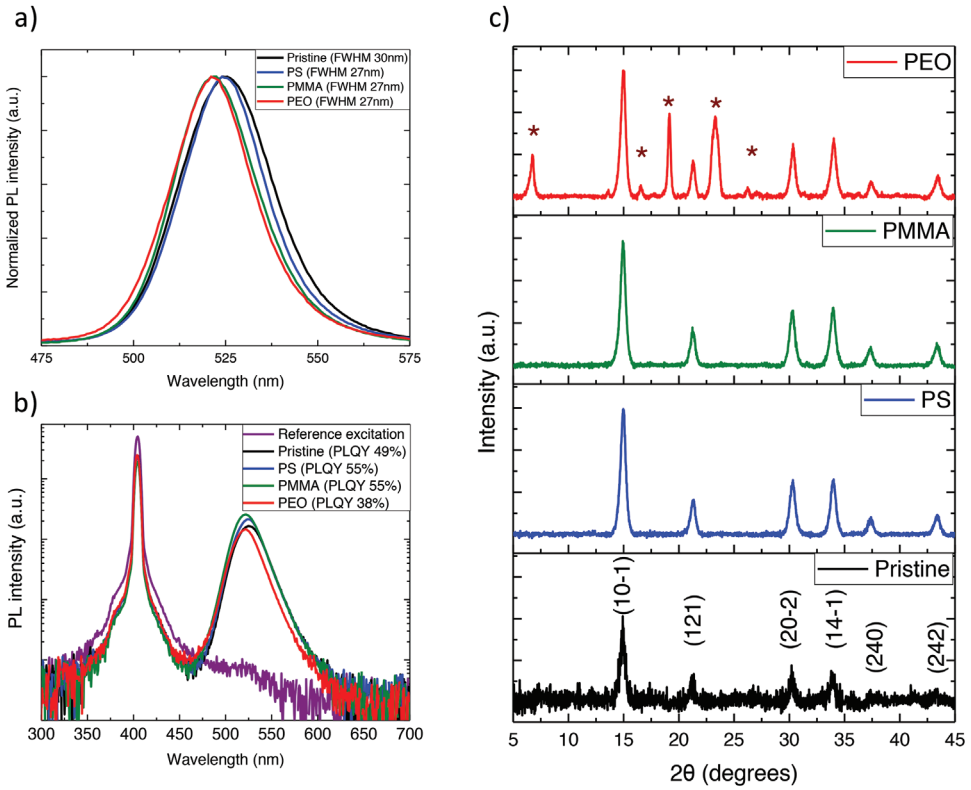

Figure 1. a) Normalized PL emission of the ball-milled powders when excited by a 405 nm laser, where pristine is the perovskite without polymer. In the legend, the FWHM of the PL is stated in nanometers. b) PLQY spectra where the powders were excited at 405 nm (reference excitation) and a spectrometer coupled to an integrated sphere from Hamamatsu was used to obtain the spectra and the PLQY. In the legend, the PLQY of the powders is stated in percentages. c) XRD pattern of the different powders. The indices display the orthorhombic perovskite diffraction peaks (ICSD collection code 158306). The asterisks at the diffraction pattern of PEO indicate the nonorthorhombic diffraction peaks.

the precursor mixture. By adjusting the stoichiometric amount of AmCl with respect to the lead(II)iodide (PbI_2) and methylammonium bromide (MABr) precursors, a PLQY as high as 29% for $MAPbBr_3$+50%AmCl was achieved.[19] In a different study, the importance of the ball-milling time with respect to the absolute PL of $CsPbBr_3$ was observed. There they noticed that prolonged ball-milling of the $CsPbBr_3$ leads to a loss of the PL.[29] Here, we return to the $MAPbBr_3$+50%AmCl perovskite formulation due to the relatively high reported PLQY. We investigate the effect of the ball-milling time on the PLQY of the resulting composition $MAPbBr_3$+50%AmCl. We found that the optimum ball-milling time is 1 h which leads to perovskite powders that have a PLQY of 49% (for more information see the Experimental Section). The perovskite powder contains a range of different particle sizes, where the smallest particles have a size of at least as small as 100 nm and the largest particles are up to ≈3 μm (see the Supporting Information Figure S1).

After the formation of the highly luminescent perovskite powders, a polymer is added to the powder. The effect of three commonly available thermoplastic polymers, PMMA, PS, and PEO was evaluated. These polymers were selected as they are transparent and are frequently used as passivation or encapsulation material for perovskites.[30–35] To ensure a thorough mixing with the previously prepared luminescent perovskite powder, these powders and the polymer were ball-milled for an additional 3 min. The optical properties of the pristine perovskite powder are compared with the perovskite powders to which the polymer was added (33 wt% $MAPbBr_3$+50%AmCl with respect to the polymer). **Figure 1**a demonstrates the normalized PL spectrum of the pristine perovskite powder which is obtained from a spectrometer equipped with an integrating sphere. The maximum of the emission spectrum is around 524 nm. Adding any of the polymers does not result in a significant shift in this maximum, but the FWHM of the PL is reduced when the polymers are introduced to the perovskite powders. In addition, the PLQY, deducted from Figure 1b, for the PS and PMMA-containing powders is increased reaching values of 55% and the PLQY of the PEO-containing powders is reduced to 38%. The increase of the PLQY and reduction of the FWHM when introducing PMMA and PS is an indication that these polymers are passivating the perovskite powder. The introduction of PEO leads to the partial quenching of the PLQY of the perovskite–polymer powder.

To study the effect of the polymers on the perovskite in more detail, structural analyses were performed. In Figure 1c, the X-ray diffraction (XRD) data reveal that the pristine perovskite powder has the expected orthorhombic perovskite diffraction peaks.[19] When ball-milling PMMA or PS with the pristine powder, the perovskite-related diffraction peaks are preserved and no extra diffraction peaks are observed. This is different for the

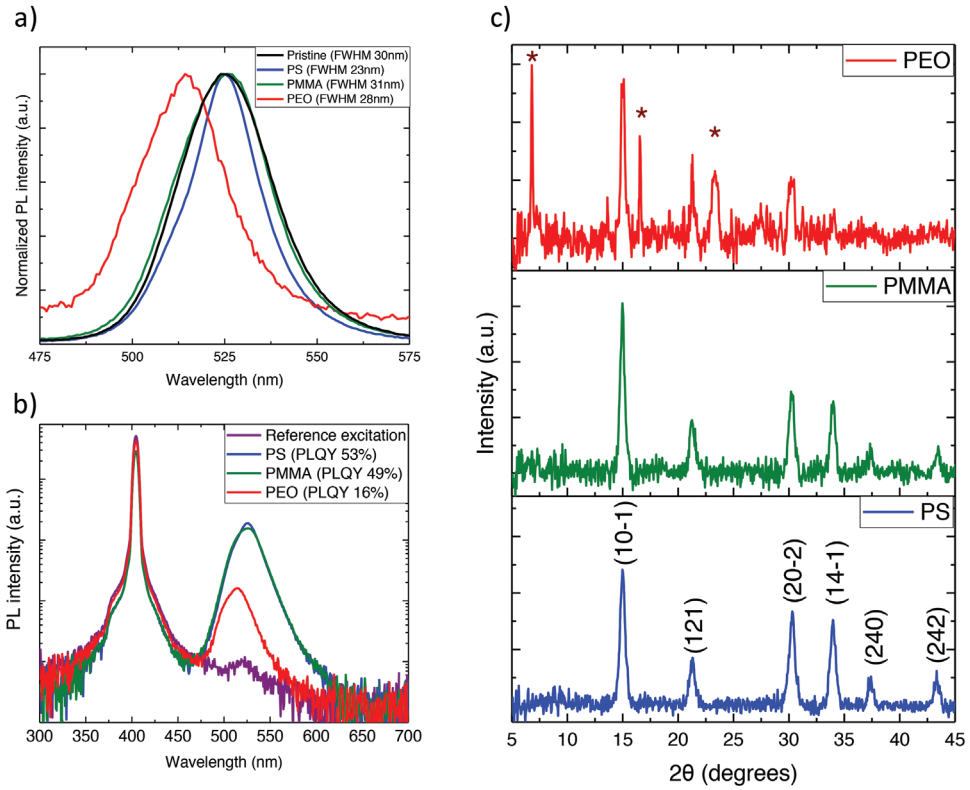

Figure 2. a) Normalized PL emission of the 33 wt% perovskite disks when excited by a 405 nm laser, where pristine is the perovskite powder without polymer. In the legend, the FWHM of the PL in nanometers is stated. b) PLQY spectra where the disks were excited at 405 nm (reference excitation) and a spectrometer coupled to an integrated sphere from Hamamatsu was used to obtain the spectra and the PLQY. In the legend, the PLQY of the disks is stated in percentages. c) XRD pattern of the different powders. The indices display the orthorhombic perovskite diffraction peaks (ICSD collection code 158306). The asterisks at the diffraction pattern of PEO indicate the nonorthorhombic diffraction peaks.

PEO-containing perovskite powders. In this case, some additional diffraction peaks appear, which is indicative of the formation of some structures different from the original orthorhombic perovskite. PEO is a known passivator for perovskites and the origin of this passivation is discussed in multiple papers.[30,36–39] The consensus is that the hygroscopic PEO is sharing the C–O lone-electron pair with the empty 6p orbital of Pb^{2+} in the perovskite, forming a Pb–O bond.[30] While this can passivate the surface of a perovskite when, e.g., PEO is spin-coated on top of a perovskite, this bonding of the PEO with the perovskite likely affects the formation of the orthorhombic perovskite phase when PEO is added during ball-milling.

To convert the powders into more useful shapes, the perovskite–polymer composite powders were processed into thin disks by heating the powder in a mold under a high pressure. The temperature during pressing was adjusted so that the powders were heated above the glass temperature of the polymer used in the composition. The thickness of the final disks was controlled through spacer rings. In the following, we focus on the disks obtained with a pressure of 1.5 metric tons. The mold temperature was set at 70 °C for the PEO-containing and at 130 °C for the PMMA and PS-containing composite powders. A spacer ring with a thickness of 25 µm is used to define the final thickness of the pressed disks, resulting in disks with a thickness between 25 and 30 µm.

In **Figure 2**a, the normalized PL spectra of the different thin disks are plotted together with that of the pristine perovskite powder. The PL spectra of the PMMA and PS-containing disks show no distinguishable shift with respect to that of the pristine perovskite powders. The PL spectrum of the PEO-containing disk shows a blue shift compared to the pristine perovskite powders. The same shift is observed in the absorbance of the disks (Figure S2, Supporting Information). Taking into account the FWHM values of the PL in Figure 2a and the PLQY values deducted from Figure 2b, of the three types of disks the one containing PS has the best optical properties, with a PLQY of around 53% and a reduced FWHM of 23 nm. The disks containing PMMA have almost the same PLQY (47%) and FWHM (31 nm) as the pristine perovskite, while the PLQY of the PEO-containing disks is reduced to a PLQY around 16% and here the FWHM is around 28 nm. To acquire more accurate PLQY and FWHM of the PL values, these measurements are repeated for different disks (Figure S3, Supporting Information). Taking into account the fact that the whole process is solvent-free and only moderate temperatures are employed for short times, these high PLQY values for perovskite disks are promising for applications.

To investigate the effect of the disk processing conditions on the perovskite composition, the XRD patterns were evaluated (Figure 2c). The PMMA and PS-containing disks have XRD patterns that are similar to those of the perovskite powders and no

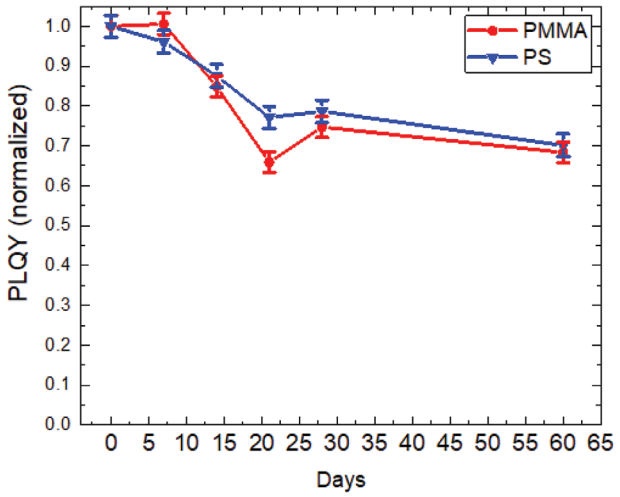

Figure 3. Normalized PLQY of the disks as a function of time in an inert atmosphere at 85 °C.

extra diffraction peaks are observed. For the PEO-containing disk, the XRD pattern demonstrates that the orthorhombic perovskite diffraction peaks are suppressed, which is especially noticeable at the higher angles. Furthermore, the additional diffraction peaks already observed when we added the PEO to the powders, became more intense. This indicates that the amount of nonorthorhombic perovskite structures increases when processing the powders into the disks. Due to these negative effects of the insertion of PEO and the processing into disk, we did not use the PEO disks for the following experiments.

The stability of the color converter is an important factor. As mentioned before, encapsulation of the perovskite by polymers can enhance the stability of the perovskite significantly. For example, in an earlier study by Hintermayr et al., methylammonium lead trihalide perovskite nanocrystals were encapsulated by polymer micelles. These encapsulated nanocrystals maintain almost 60% of the initial PL after 130 days in ambient conditions, whereas the noncapsulated nanocrystals degraded completely in 13 days.[40] A common method to measure the stability is to monitor the PLQY value of the color converter over time under different conditions.[41] One of the frequently used stressing conditions is the stability of the color converter under ambient air conditions. Under these conditions for 62 days, the fabricated disks with PS and PMMA maintain 83% and 77%, respectively, of the initial PLQY. As a comparison, the PLQY of the pristine perovskite powder without the added polymer dropped to 26% of the initial value in just 7 days under ambient conditions. These results indicate that this solvent-free method can encapsulate the perovskite in a PS or PMMA surrounding which protects the perovskite from ambient conditions. It is interesting to observe that with this process PMMA is protecting the perovskite from external conditions since PMMA is not able to protect the perovskite when the film is processed in solution by using the swelling/deswelling method.[42]

Another common stability test is to put the disks at elevated temperatures. We kept the disks at 85 °C in an inert atmosphere (N_2) and determined the PLQY loss at set time intervals. **Figure 3** shows the normalized PLQY as a function of time at 85 °C. Both disks show a similar PLQY degradation and maintain some 70% of the initial values after 2 months at 85 °C. Interestingly, the speed of degradation reduces over time. There is a strange partial recovery of the PLQY around day 28, which is not quite understood. It could be related to N_2-induced lattice recovery as was reported elsewhere.[43] These stability tests demonstrate that the color converters are rather stable at elevated temperatures. It is known that PMMA can passivate under-coordinated Pb^{2+} ions, whereas PS is reported to passivate surface defects.[32,44–46] Overall, the increase in PLQY and the prolonged stability of the PS and PMMA-containing disks imply that the addition of these polymers lead to the passivation of defects that reduce trap states.

The disks that we described so far, containing 33 wt% $MAPbBr_3$+50%AmCl (with respect to the polymer) are opaque. Hence, they can only reflect light as a color converter. It is more interesting to have semitransparent color converters. This can be achieved by reducing the perovskite content with respect to the polymer. We used the PMMA-based disks to verify the optimum perovskite concentration in the polymer matrix. Disks were prepared with 0.5, 1, and 2 wt% of perovskite with respect to PMMA. The PLQY of the disks with 0.5 and 1 wt% is roughly half of that of the opaque films (**Figure 4**a). The disks with 2 wt% had a similar PLQY as the opaque films with the 33 wt% perovskite with respect to PMMA. The transmittance of the films reduces with increasing perovskite concentration and therefore, we did not go beyond the 2 wt% perovskite loading. The transmittance for wavelengths beyond the absorption edge of the perovskite increases significantly reaching 72% at 600 nm for the disk containing 2 wt% perovskite in PMMA (Figure 4b). We infer the transmittance for these disks by carefully measuring their reflectance. The disks are excited by a deuterium halogen source and the reflected light is collected by an integrating sphere. Since there is no absorption from the perovskite in the region where the wavelength energy of the incoming light is lower than the bandgap of the perovskite, the transmittance can be retrieved. For more information on the experimental procedure, see the Experimental Section.

We now compare the properties of the semitransparent and the opaque disks. The disks with a perovskite concentration of 2 wt% are semitransparent (**Figure 5**a,b) whereas those with 33 wt% are almost completely opaque for the disks with thicknesses of 30 µm (Figure 5c,d). The disks with 33 wt% perovskite in PMMA and PS have a transmittance for wavelengths with lower energy than the bandgap of the perovskite of 16% and 30%, respectively (Figure 5e). The low transmittance in this range of wavelengths is due to the high reflection of the disks. The transmittance in this wavelength range increases when the content of the perovskite is reduced to 2 wt%, resulting in a transmittance of above 72% and 75% for the PMMA and PS-containing disks, respectively. The PLQY of the disk with the 2 wt% perovskite in PMMA is 48%, hence similar to what was observed for the more concentrated disks. The FWHM for the 2 wt% perovskite-containing disks, however, is reduced to a value of ±20.5 nm. Hence, the reduction of the perovskite content improves the color purity without reducing the PLQY of the disks. For the PS-based disk with 2 wt% perovskite, the PLQY increases to 60% and the FWHM is 21 nm, showing an improvement in optical properties, compared with the more concentrated perovskite PS disks. This hints at better passivation of the perovskite when increasing

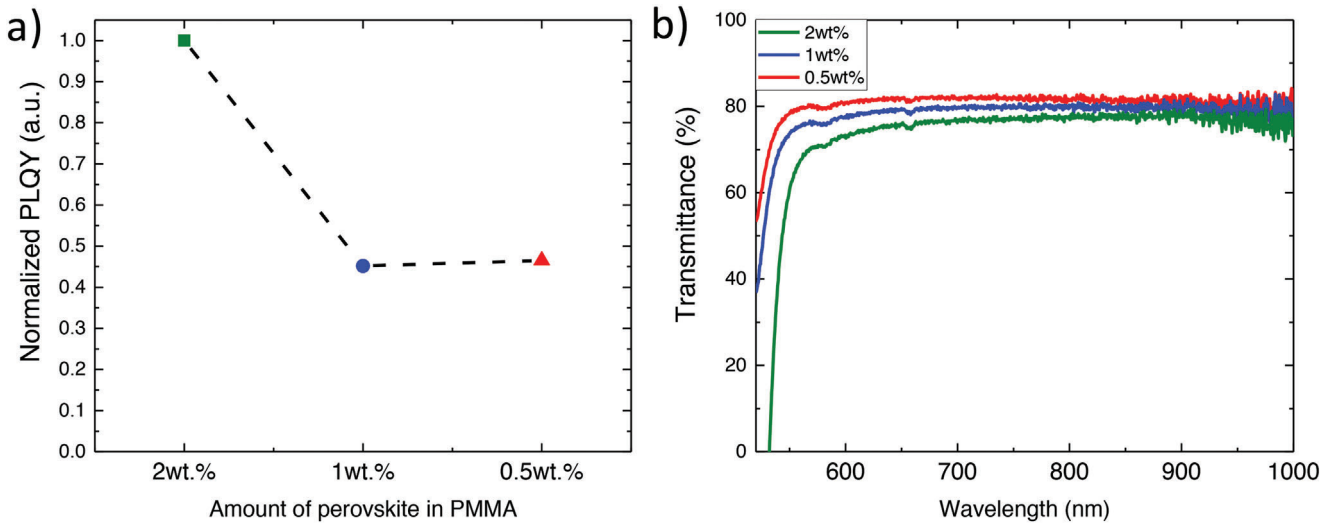

Figure 4. Optical properties of PMMA disks containing a low amount of the luminescent perovskites, 0.5, 1, and 2 wt% with respect to PMMA. a) Normalized PLQY with respect to the PLQY of the 33 wt% PMMA disk as a function of perovskite concentration. b) Transmittance as a function of wavelength and perovskite concentration.

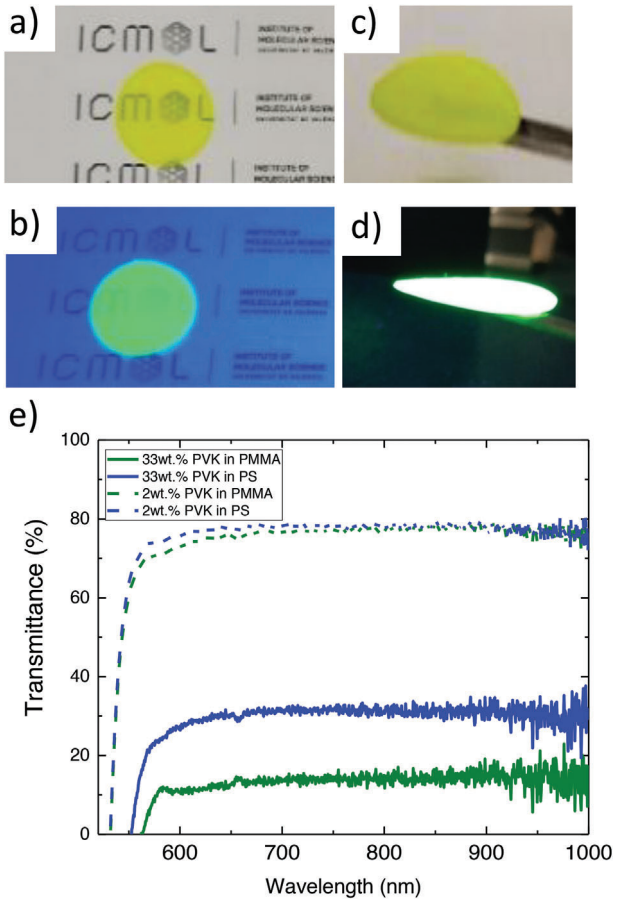

Figure 5. Photographs of PMMA disks containing a,b) 2 and c,d) 33 wt% under ambient light and UV illumination (365 nm), respectively. e) Transmittance data for PMMA and PS disk with different concentrations of perovskites.

the polymer to perovskite ratio. In Figure S4 in the Supporting Information, the statistical distribution of the PLQY and FWHM of these disks is plotted. The width of the distribution of the properties is rather narrow demonstrating the good reproducibility of this dry fabrication process. Higher PLQYs reaching 75% were obtained when some of the disks were stressed at 85 °C for several weeks in an inert N_2 atmosphere. We do not yet know the origin of this increase in PLQY but decided to mention it here regardless.

As mentioned, an additive such as AmCl can easily be incorporated into the perovskite–polymer complex since the process does not rely on solvents, and only moderate temperatures are used for a short period. As a proof of concept, we also prepared a multiple-color converter by inserting in addition to the perovskite powder a fluorescent polymer. We used a commercial polyfluorene-based polymer named RedF from Sumitomo Chemical. RedF is selected because it emits in the lower energy wavelengths, complementary to the emission spectra of the 2 wt% $MAPbBr_3$+50%AmCl perovskite. Moreover, the disks have a high transmittance in the wavelength region where RedF emits. Importantly, RedF absorbs around the wavelength where the perovskite emits (see Figure S5, Supporting Information). Therefore, a low concentration of 2 wt% RedF is selected, so the parasitic absorption of the RedF on the perovskite is reduced. The RedF is added to the PMMA and perovskite powder followed by 3 min of ball-milling. Accordingly, the powder mixture contains two light-emitting materials where $MAPbBr_3$+50%AmCl converts the incident blue light to green and RedF converts the incident blue light to red. This dual-emitter color converter is a simpler alternative to the frequently used stacked layers of two color converters.[47–49] Similarly as before, the powders are pressed into a thin disk. For comparison reasons, a RedF-only containing disk in PMMA is also prepared. In **Figure 6**a, the PL spectra of this disk and the previously studied one containing only the perovskite composite are depicted. We can see that the emission spectrum of the dual emitter disks perfectly overlaps

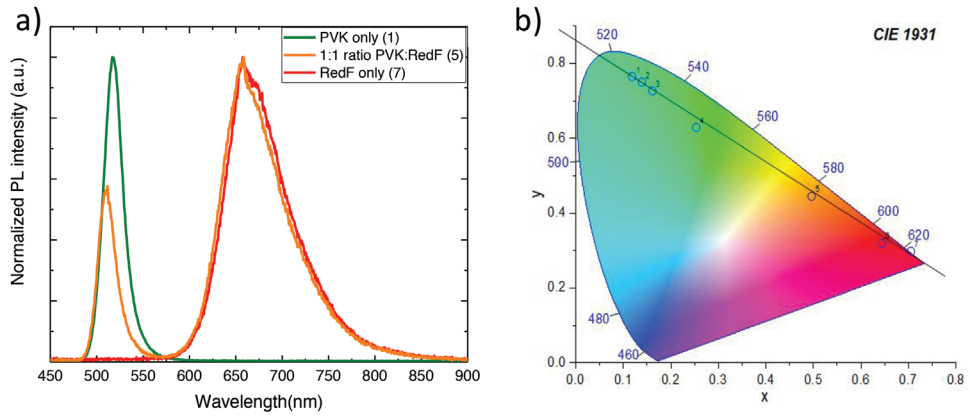

Figure 6. a) Photoluminescence spectra of disks containing perovskite (PVK), Red F, and both at an individual concentration of 2 wt% with respect to PMMA. b) Color points depicted in the CIE 1931 graph from disks containing both 2 wt% Red F and the 2 wt% perovskite emitter in different ratios. Point numbers 1 to 7 have the following ratios of 2 wt% PVK: 2 wt% RedF: 1) PVK only, 2) 99:1, 3) 90:10, 4) 67:33, 5) 50:50, 6) 33:67 and as last number 7) with only 2 wt% RedF.

with the emission of both types of disks with only one of the two emitters. The PLQY of the perovskite and RedF-only color converters is 48% and 60%, respectively. When combining the two light-emitting materials, an orange color converter with a final PLQY of around 42% is produced. The decrease in PLQY is likely due to the partial reabsorption of the converted green light by the RedF emitter.

Another way to specify the color converters is to look at their color points as represented in the CIE 1931 graph (Figure 6b). The color points were obtained from the emission spectra of the disks. The RedF-only (number 7) and perovskite-only (number 1) disks have color points lying at the extreme red and green of the CIE1931 graph. The color coordinates of the perovskite-only-based disk are very close to the ideal green Rec 2020 standard. This implies that if the color coordinates of the perovskite emitter would be used for the green part of the Rec 2020, still >98% of the color gamut could be reproduced.[50,51] Disks that contain both the perovskite and RedF emitters have color points that fall on a linear line between the two single emitter-containing disks. This demonstrates the adaptability of this process. The above-described results show that with this synthesis method, it is possible to successfully produce a multiple (colored) color converter.

3. Conclusion

Polymeric disks containing highly luminescent perovskite emitters are prepared using a solvent-free process. We add powders of some well-known polymers to a previously mechanochemical synthesized luminescent $MAPbBr_3$ perovskite formulation. PMMA and PS are compatible with the perovskite and improved their luminescent properties reaching PLQYs above 50%. Incorporating PEO in the perovskite powder results in a reaction with the bulk of the perovskite leading to a partial reduction of the PLQY. As luminescence polymer–perovskite powders do not have a form factor compatible with most applications, we converted the powders into thin disks. Surprisingly, by applying moderate temperature and pressure, it is possible to press the powders into thin disks while maintaining the luminescent properties and improving the stability. Hence, the presence of PMMA and PS improves the properties and allows the formation of mechanically robust disks. Depending on the perovskite content, semitransparent or opaque luminescent disks are obtained. Using a disk composition with 33 wt% perovskite led to an opaque disk with a PLQY of around 53% and an FWHM of around 23 nm for the PS-containing disks and a PLQY of around 48% and an FWHM of around 28 nm for the PMMA-holding disk. Reducing the wt% of the perovskite to 2% led to color converters with a PLQY of 60% and an FWHM as low as 21 nm for the PS. These properties make these disks excellent candidates for color converters as they have a very high color purity and high luminescence. The transmittance of these disks for wavelengths greater than 600 nm was above 72% and 75% for the PMMA and PS holding disks, respectively. A proof of concept dual green and red light-emitting color converting disk was also prepared by adding a fluorescent polymer to the perovskite during the mechanochemical synthesis and subsequent pressing at elevated temperatures. The advantages of this dry process technology pave the way toward productive polymer-embedded perovskite color converter fabrication.

4. Experimental Section

Materials: Methylammonium bromide (MABr, >99.5%) was purchased from Lumtec. Lead(II) bromide ($PbBr_2$, ≥98%) was purchased from TCI. Amantadine hydrochloride was purchased from Sigma-Aldrich. RedF was purchased from Sumitomo Chemical. All chemicals were stored in a nitrogen-filled glovebox and used as received without further purification. The polymers PMMA, PEO, and PS were purchased from Sigma-Aldrich.

Preparation of Perovskite Powder and Perovskite Polymer Mixture: To produce the color converter, first, an appropriate perovskite was selected with a high PLQY and a desired wavelength in the visible range. For this work, $MAPbBr_3$+50%AmCl was used which was developed previously. To produce the perovskite, the precursors (1 mmol of MABr, 1 mmol of $PbBr_2$, and 0.5 mmol of AmCl) were introduced and closed inside a 10 mL zirconia ball-mill jar with two zirconia beads of 10 mm in diameter under ambient atmosphere. Then ball-milling (mechanochemical synthesis) was performed with an MM-400 straight ball mill from Retsch, at a frequency of

30 Hz for 1 h. By reducing the time of ball-milling with a fixed frequency of 30 Hz to 1 h, the PLQY of the perovskite increased from the previously published value of 29% to 49%. Further reduction of the ball-milling time did not lead to the full conversion of the precursors into the perovskite configuration.

After the perovskite was formed, one of the selected polymers (PMMA, PS, or PEO) was added as a fine powder at the desired concentration. The pre-formed perovskite and the polymer powders were ball-milled for an additional 3 min to obtain a good mixture of the polymer and the perovskite. It is noteworthy that the perovskite powder and the mixed powders were not further processed to reduce or uniform the size of the particles. It was key to add the polymers after forming the perovskite because adding the polymer with the initial perovskite precursors resulted in low luminescent perovskite powders and additional diffraction peaks in the XRD pattern which were not in agreement with the orthorhombic perovskite phase (see Figure S6, Supporting Information). Reducing the perovskite content below 2 wt% resulted in a decrease in the PLQY in the final disk (see Figure 5a).

Fabrication of the Disks: Disks were pressed by heating the pre-formed perovskite–polymer powder mixtures in a high-pressure mold. A mold from Specac referred to in their catalog as "The Atlas constant thickness filmmaker" and the following temperature source the "Atlas series heated platens" was used. In order not to damage the polished mold, the temperature of the mold was set above the glass temperature of the used polymer. Different thicknesses of the disks, as low as 15 µm, could be achieved by introducing different spacer rings between the mold and the press. For PMMA and PS, the disks were pressed at a temperature of 130 °C whereas the PEO was pressed at 70 °C.

For the experiments in this report, the mold was pre-heated before adding the perovskite–polymer mixture. Then a short pressing time of 10 s and a pressure of 1.5 metric tons were used to reproducibly fabricate a disk. After pressing for this duration, the pressure was released and the disks were immediately removed from the hot mold. This whole process from powder to disk was performed under ambient conditions.

Structural and Spectroscopic Analyses: XRD was measured with a Panalytical Empyrean diffractometer equipped with CuKα anode operated at 45 kV and 40 mA and a Pixel 1D detector in scanning line mode. Single scans were acquired in the 2 thetas = 10° to 50° range in Bragg-Brentano geometry in air.

PLQY measurements were performed with a UV-VIS-NIR Absolute Photoluminescence Quantum Yield Spectrometer C13534-11.

The transmittance of the disks was measured in reflectance mode using the Avantes AvaLight DH-S-BAL deuterium halogen source connected with an Avantes reflection integrating sphere and collected by the Avantes AvaSpec-2048L spectrometer. To measure the reflectance, the disk was positioned on a black surface (substrate holder), and therefore transmitted light through the disk would not reflect and contribute to the collected light. In the wavelength region where the incoming light has lower energy than the bandgap energy of the perovskite, no absorption of the perovskite occurred and the transmittance in this region could be calculated from the reflectance measurement since $A+R+T = 1$ and $A = 0$. To confirm if the assumption that there was no absorption ($A = 0$) in this region was valid, another experiment in reflection was performed with the disk. There the substrate holder was not black but reflective. In this mode, all the incoming light lower than the bandgap energy of the perovskite should be reflected since the transmitted light was then also participating in the collected light, and this region of wavelengths $R+T = 1$. Indeed, with this setup, near unity (>95%) reflectance was measured confirming that the assumption of $A = 0$ in this region of wavelengths was valid and the transmittance of the disk could be calculated by measuring the reflectance.

Supporting Information

Supporting Information is available from the Wiley Online Library or from the author.

Acknowledgements

The authors gratefully acknowledge the financial support of the European Research Council (ERC) under the European Union's Horizon 2020 research and innovation program (Grant Agreement no. 834431), the Spanish Agencia Estatal de Investigaciones (AEI) project CEX2019-000919-M funded by MCIN/AEI/10.13039/501100011033, and project PID2021-126444OB-I00 funded by MCIN/AEI/10.13039/501100011033 and by "ERDF A way of making Europe".

Conflict of Interest

The authors declare no conflict of interest.

Data Availability Statement

The data that support the findings of this study are available from the corresponding author upon reasonable request.

Keywords

color converter, dry synthesis, halide perovskites, solvent free

Received: January 4, 2023
Revised: May 16, 2023
Published online: June 7, 2023

[1] F. Deschler, M. Price, S. Pathak, L. E. Klintberg, D.-D. Jarausch, R. Higler, S. Hü, T. Leijtens, S. D. Stranks, H. J. Snaith, M. Atatü, R. T. Phillips, R. H. Friend, *J. Phys. Chem. Lett.* **2014**, *5*, 1421.
[2] L. Protesescu, S. Yakunin, M. I. Bodnarchuk, F. Krieg, R. Caputo, C. H. Hendon, R. X. Yang, A. Walsh, M. V Kovalenko, *Nano Lett.* **2015**, *15*, 3692.
[3] Z. Song, J. Zhao, Q. Liu, *Inorg. Chem. Front.* **2019**, *6*, 2969.
[4] N. Sakai, B. Wenger, *Dig. Tech. Pap. – Soc. Inf. Disp. Int. Symp.* **2021**, *52*, 892.
[5] G. Lozano, *J. Phys. Chem. Lett.* **2018**, *9*, 3987.
[6] K. Ji, M. Anaya, A. Abfalterer, S. D. Stranks, *Adv. Opt. Mater.* **2021**, *9*, 2002128.
[7] Y. H. Kim, S. Kim, S. H. Jo, T.-W. Lee, *Small Methods* **2018**, *2*, 1800093.
[8] Helio Display Materials, Why Next Generation TVs Need Perovskites, https://www.heliodisplaymaterials.com (accessed: November 2022).
[9] T. Guner, M. M. Demir, *Phys. Status Solidi* **2018**, *215*, 1800120.
[10] H. Lee, J. Park, S. Kim, S. C. Lee, Y. H. Kim, T. W. Lee, *Adv. Mater. Technol.* **2020**, *5*, 2000091.
[11] E. Radicchi, E. Mosconi, F. Elisei, F. Nunzi, F. De Angelis, *ACS Appl. Energy Mater.* **2019**, *2*, 3400.
[12] L. Yuan, R. Patterson, X. Wen, Z. Zhang, G. Conibeer, S. Huang, *J. Colloid Interface Sci.* **2017**, *504*, 586.
[13] A. Pan, B. He, X. Fan, Z. Liu, J. J. Urban, A. P. Alivisatos, L. He, Y. Liu, *ACS Nano* **2016**, *10*, 7943.
[14] J. De Roo, M. Ibáñez, P. Geiregat, G. Nedelcu, W. Walravens, J. Maes, J. C. Martins, I. Van Driessche, M. V. Kovalenko, Z. Hens, *ACS Nano* **2016**, *10*, 2071.
[15] Z. Y. Zhu, Q. Q. Yang, L. F. Gao, L. Zhang, A. Y. Shi, C. L. Sun, Q. Wang, H. L. Zhang, *J. Phys. Chem. Lett.* **2017**, *8*, 1610.
[16] L. Wang, D. Ma, C. Guo, X. Jiang, M. Li, T. Xu, J. Zhu, B. Fan, W. Liu, G. Shao, H. Xu, H. Wang, R. Zhang, H. Lu, *Appl. Surf. Sci.* **2021**, *543*, 148782.
[17] P. Sadhukhan, S. Kundu, A. Roy, A. Ray, P. Maji, H. Dutta, S. K. Pradhan, S. Das, *Cryst. Growth Des.* **2018**, *18*, 3428.

[18] Z. Hong, D. Tan, A. John, N. Mathews, F. García, H. Sen Soo, *iScience* **2019**, *16*, 312.
[19] L. Martínez-Sarti, F. Palazon, M. Sessolo, H. J. Bolink, *Adv. Opt. Mater.* **2020**, *8*, 1901494.
[20] D. Prochowicz, P. Yadav, M. Saliba, M. Saski, S. M. Zakeeruddin, J. L. Lewiński, M. Grä, *ACS Appl. Mater. Interfaces* **2017**, *9*, 28418.
[21] M. A. Van De Haar, M. Tachikirt, A. C. Berends, M. R. Krames, A. Meijerink, F. T. Rabouw, *ACS Photonics* **2021**, *8*, 1784.
[22] K. A. Bush, C. D. Bailie, Y. Chen, A. R. Bowring, W. Wang, W. Ma, T. Leijtens, F. Moghadam, M. D. McGehee, *Adv. Mater.* **2016**, *28*, 3937.
[23] S. Shi, L. Cao, H. Gao, Z. Tian, W. Bi, C. Geng, S. Xu, *Nanoscale* **2021**, *13*, 9381.
[24] X. Li, X. Qu, Z. Wen, B. Xu, K. Wang, X. W. Sun, *Dig. Tech. Pap. – Soc. Inf. Disp. Int. Symp.* **2020**, *51*, 1775.
[25] J. Xue, Y. Gu, Q. Shan, Y. Zou, J. Song, L. Xu, Y. Dong, J. Li, H. Zeng, *Angew. Chemie* **2017**, *129*, 5316.
[26] N. Sakai, H. Hopkin, G. De Keyzer, B. Wenger, *Dig. Tech. Pap. Soc. Inf. Disp. Int. Symp.* **2022**, *53*, 307.
[27] Z. Nie, E. Kumacheva, *Nat. Mater.* **2008**, *7*, 277.
[28] L. J. Guo, *Adv. Mater.* **2007**, *19*, 495.
[29] F. Palazon, Y. El Ajjouri, P. Sebastia-Luna, S. Lauciello, L. Manna, H. J. Bolink, *J. Mater. Chem. C* **2019**, *7*, 11406.
[30] M. Kim, S. G. Motti, R. Sorrentino, A. Petrozza, *Energy Environ. Sci.* **2018**, *11*, 2609.
[31] L. Song, X. Guo, Y. Hu, Y. Lv, J. Lin, Z. Liu, Y. Fan, X. Liu, *J. Phys. Chem. Lett.* **2017**, *8*, 4148.
[32] M. Li, X. Yan, Z. Kang, Y. Huan, Y. Li, R. Zhang, Y. Zhang, *ACS Appl. Mater. Interfaces* **2018**, *10*, 18787.
[33] Y. Wei, X. Deng, Z. Xie, X. Cai, S. Liang, P. Ma, Z. Hou, Z. Cheng, J. Lin, *Adv. Funct. Mater.* **2017**, *27*, 1703535.
[34] F. Corsini, G. Griffini, *J. Phys. Energy* **2020**, *2*, 031002.
[35] J. Peng, J. I. Khan, W. Liu, E. Ugur, T. Duong, Y. Wu, H. Shen, K. Wang, H. Dang, E. Aydin, X. Yang, Y. Wan, K. J. Weber, K. R. Catchpole, F. Laquai, S. De Wolf, T. P. White, *Adv. Energy Mater.* **2018**, *8*, 1801208.
[36] S. G. Motti, D. Meggiolaro, A. J. Barker, E. Mosconi, C. A. R. Perini, J. M. Ball, M. Gandini, M. Kim, F. De Angelis, A. Petrozza, *Nat. Photonics* **2019**, *13*, 532.
[37] Y. Ling, Y. Tian, X. Wang, J. C. Wang, J. M. Knox, F. Perez-Orive, Y. Du, L. Tan, K. Hanson, B. Ma, H. Gao, *Adv. Mater.* **2016**, *28*, 8983.
[38] P. Qin, T. Wu, Z. Wang, X. Zheng, X. Yu, G. Fang, G. Li, *Sol. RRL* **2019**, *3*, 1900134.
[39] Z. Wang, Z. Luo, C. Zhao, Q. Guo, Y. Wang, F. Wang, X. Bian, A. Alsaedi, T. Hayat, Z. Tan, *J. Phys. Chem. C* **2017**, *121*, 28132.
[40] V. A. Hintermayr, C. Lampe, M. Löw, J. Roemer, W. Vanderlinden, M. Gramlich, A. X. Böhm, C. Sattler, B. Nickel, T. Lohmüller, A. S. Urban, *Nano Lett.* **2019**, *19*, 4928.
[41] Y. Wei, Z. Cheng, J. Lin, *Chem. Soc. Rev.* **2019**, *48*, 310.
[42] Y. Wang, J. He, H. Chen, J. Chen, R. Zhu, P. Ma, A. Towers, Y. Lin, A. J. Gesquiere, S. T. Wu, Y. Dong, *Adv. Mater.* **2016**, *28*, 10710.
[43] A. Alberti, I. Deretzis, G. Mannino, E. Smecca, F. Giannazzo, A. Listorti, S. Colella, S. Masi, A. L.a Magna, *Adv. Energy Mater.* **2019**, *9*, 1803450.
[44] J. Peng, J. I. Khan, W. Liu, E. Ugur, T. Duong, Y. Wu, H. Shen, K. Wang, H. Dang, E. Aydin, X. Yang, Y. Wan, K. J. Weber, K. R. Catchpole, F. Laquai, S. De Wolf, T. P. White, *Adv. Energy Mater.* **2018**, *8*, 1801208.
[45] Y. Li, M. Dailey, P. J. Lohr, A. D. Printz, *J. Mater. Chem. A* **2021**, *9*, 16281.
[46] J. Chen, X. Huang, Z. Xu, Y. Chi, *ACS Appl. Mater. Interfaces* **2022**, *14*, 33703.
[47] Y. Peng, Q. Sun, J. Liu, H. Cheng, Y. Mou, *J. Alloys Compd.* **2021**, *850*, 156811.
[48] Z. Lin, H. Lin, J. Xu, F. Huang, H. Chen, B. Wang, Y. Wang, *J. Alloys Compd.* **2015**, *649*, 661.
[49] H. W. Choi, K. N. Hui, P. T. Lai, X. H. Wang, Z. L. Li, *Opt. Express* **2009**, *17*, 9873.
[50] ITU, *Parameter Values for Ultra-high Definition Television Systems for Production and International Programme Exchange*, International Telecommunication Union, Geneva, Switzerland **2015**.
[51] M. Sugawara, S. Y. Choi, D. Wood, *IEEE Signal Process. Mag.* **2014**, *31*, 170.